Optical Materials 49 (2015) 249–254

Contents lists available at ScienceDirect

Optical Materials

journal homepage: www.elsevier.com/locate/optmat

Effect of lead fluoride incorporation on the structure and luminescence properties of tungsten sodium phosphate glasses

Rachel Prado Russo Delorenzo Nardi [a], Celso Eduardo Braz [a], Andrea S.S. de Camargo [b], Sidney J.L. Ribeiro [c], Lucas A. Rocha [d], Fábia Castro Cassanjes [a], Gael Poirier [a,*]

[a] Grupo de Química de Materiais, Universidade Federal de Alfenas, Campus de Poços de Caldas, Poços de Caldas, MG, Brazil
[b] Instituto de Física de São Carlos, Universidade de São Paulo, São Carlos, SP 13566-590, Brazil
[c] Instituto de Química, Universidade Estadual Paulista Júlio de Mesquita Filho, Araraquara, SP, Brazil
[d] Universidade de Franca – UNIFRAN – CP-82, Franca, SP 14404-600, Brazil

ARTICLE INFO

Article history:
Received 13 June 2015
Received in revised form 15 August 2015
Accepted 8 September 2015
Available online 25 September 2015

Keywords:
Glass
Phosphate
Tungsten
Lead fluoride
Europium

ABSTRACT

Tungsten phosphate glasses are known to be promising materials for several applications in optics such as non linear optical properties, lower phonon energy or photochromic effects related with tungsten oxide incorporation inside the phosphate network. In this study, lead fluoride has been incorporated in a $60NaPO_3$–$40WO_3$ glass composition according to the ternary molar compositions $(100-x)[0.6NaPO_3$–$0.4WO_3]$–$xPbF_2$ with x varying from 0 to 60 mol%. The structural changes as a function of composition were investigated by thermal analysis, UV–visible absorption, Raman spectroscopy, X-ray diffraction of the crystallized samples, and Eu^{3+} emission in the visible. While DSC analyzes points out a strong decrease in the glass network connectivity and higher crystallization tendency with increasing PbF_2 contents, Raman spectra clearly identify a progressive incorporation of PbF_2 in the phosphate network with the formation of terminal P—F and W—F bonds. These results are also in agreement with the crystallization of β-PbF_2 observed for the most lead fluoride concentrated samples. Investigation of Eu^{3+} emission data in the visible showed longer $^5D_0$ excited state lifetime values and higher quantum efficiencies. These results are discussed in terms of the assumption of higher local symmetry around Eu^{3+} with increasing PbF_2 contents.

1. Introduction

Tungsten phosphate glasses have been extensively investigated in the past few years because of new thermal, physical and optical properties obtained from the insertion of WO_6 polyhedra inside the covalent phosphate chains [1–3]. Such specific properties, not observed in classical phosphate glasses, include extremely high thermal stability against devitrification [4], non linear optical absorption [5,6], photochromic effects under visible irradiation [7–9] and/or efficient emission properties of rare earth (RE) ions [10]. In fact, the incorporation of tungsten oxide, which behaves as a glass intermediary in the phosphate covalent network, results in progressively higher polymerization and higher connectivity related with the insertion of WO_6 units between the phosphate PO_4 tetrahedra, which cross-link the phosphate chains. This highly connected glass structure exhibits high viscosity near the melting temperature, hindering crystallization events and lowering phonon energies when compared to classical phosphates glasses [1–3]. For these reasons, tungsten phosphate glasses are suitable hosts for other glass modifier incorporation such as metallic halides or rare earth salts.

On the other hand, oxyfluoride glasses also present very promising characteristics as rare earth ion hosts since they combine physical properties of both oxides (high glass forming ability, thermal stability, easy preparation and high RE solubility) and fluorides compounds (low phonon energy and refractive index) [11–14]. Luminescent properties are improved when heavy metal fluoride nanocrystallites are precipitated from the precursor glass matrix since rare earth ions usually migrate to the low phonon energy crystalline phase [15–24]. However, incorporation of large amounts of heavy metal fluorides is often difficult since its modifier behavior usually highly depolymerizes the glass network with an increasing tendency of the resulting melt to crystallize upon cooling.

In this work, we investigated the ability of the glass composition $60NaPO_3$–$40WO_3$, which is known for its very high thermal

* Corresponding author at: Instituto de Ciência e Tecnologia, Campus de Poços de Caldas, Caldas, MG 37715-400, Brazil.
E-mail address: gael.poirier@unifal-mg.edu.br (G. Poirier).

http://dx.doi.org/10.1016/j.optmat.2015.09.008
0925-3467/

stability, to incorporate increasing contents of lead fluoride PbF_2. Glass forming ability under melt-quenching condition has been studied in the ternary system $(100 - x)[0.6NaPO_3–0.4WO_3]–xPbF_2$ in order to determine the highest PbF_2 content without devitrification. Afterwards, the work focuses on the structural evolution of the glass network as a function of the lead fluoride content using thermal analysis, UV–visible absorption, Raman spectroscopy, Eu^{3+} emission in the visible and X-ray diffraction of some crystallized glass samples.

2. Experimental part

Glass samples were prepared using the classical melt-quenching method: the starting powders NaH_2PO_4 99.9%, WO_3 99.99%, PbF_2 99.9% and Eu_2O_3 99.999% from Aldrich were weighted, grinded in an agate mortar and introduced in a covered platinum crucible. The crucible was heated from room temperature to 850 °C at 20 °C/min and kept at this temperature for 10 min for samples with $x = 0$, 10, 20, 30 whereas samples with $x = 40$, 50, 60 were melted at 800 °C. These low melting temperatures and times were chosen in order to minimize the fluorine loss by evaporation of the melt. Sample weight before and after melting allowed determination of a weight loss around 0.5%. Then, the melt was quenched in a steel mold preheated 20 °C below the glass transition temperature and kept at this temperature for 4 h before undergoing slow cooling to room temperature inside the furnace. The glass samples were polished for optical characterizations. Eu^{3+}-doped glass samples were prepared using the same methodology by adding 0.1 mol% of Eu_2O_3 to the starting powder precursors. DSC measurements were performed on bulk samples between 150 °C and 550 °C at a heating rate of 10 °C/min in sealed aluminum pans under N_2 using a flow of 50 mL/min. The calorimeter used for these characterizations is a DSC 200 F3 Maia from Netzsch. UV–visible absorption spectra were recorded between 190 nm and 550 nm at 1 nm/s using a Hach DR3900 spectrophotometer. Band-gap energy of glass samples were determined using the method described earlier and based on the Tauc law [25]. Raman spectra were measured for undoped bulk glass samples between 100 cm^{-1} and 1200 cm^{-1} using a LabRam Micro-Raman from Horiba Jobin–Yvon, working at an excitation wavelength of 632.8 nm (He–Ne laser). The photoluminescence emission spectra of the Eu^{3+}-doped samples were measured in a HORIBA Jobin Yvon spectrofluorimeter model Fluorolog FL3-221, equipped with CW xenon flash lamp and a photomultiplier detector (HORIBA PPD-850). The excited state lifetime values of Eu^{3+} ($^5D_0$ state) were determined by exponentially fitting the PL decay curves using a pulsed flash lamp. X-ray diffraction measurements were performed on powder samples using a Rigaku ultima IV diffractometer working at 40 kV and 30 mA between 10° and 70° in continuous mode of 0.02°/s. The crystalline phases were identified according to X-ray powder diffraction patterns (PDF file) [26].

3. Results and discussion

Glass samples were successfully obtained by the melt-quenching method in the ternary system $(100 - x)[0.6NaPO_3–0.4WO_3]–xPbF_2$ with x varying from 0 to 60 mol%. Eu^{3+}-doped glasses were obtained with $x = 0$–40% whereas higher lead fluorine contents induce sample devitrification. The $NaPO_3/WO_3$ molar ratio was kept constant because of the well-known extremely high chemical and thermal stability of the glass composition $60NaPO_3–40WO_3$ [3,4]. Low melting temperature and short melting time were used in order to minimize the fluorine loss and a mass loss of about 0.5% has been estimated after melting. However, fluorine loss related with reaction with water and HF loss has already been reported in other works and the final fluorine molar content must be verified by ^{19}F NMR and electrochemical methods. Increasing lead fluorine contents resulted in very distinct glasses with loss of the characteristic dark coloration observed for $x = 0$ and $x = 10$ (Fig. 1) and a strong decrease of the melt viscosity observed during the casting process. The strong absorption in the visible, already reported in tungsten phosphate glasses [9], is commonly attributed to reduced tungsten species W^{5+} and W^{4+} in tungsten oxide rich domains built up from WO_6 clusters. For this reason, these compositions only exhibit the tungsten reduction in WO_3 concentrated samples since these WO_6 clusters seem to stabilize the reduced tungsten ions. Based on these structural considerations, the increasing glass transparency with increasing lead fluoride content gives the first evidence that these tungsten oxide clusters are progressively dismantled by the fluoride incorporation. The lower viscosity is another indication that the covalent glass network is being modified. By all means, these experimental observations are in agreement with an effective incorporation of PbF_2 in the glass network.

DSC curves obtained on bulk samples are presented in Fig. 2 from $x = 0$ to $x = 60$ and the characteristic temperatures such as glass transition and the first crystallization event are resumed in Table 1, together with the thermal stability parameter $Tx_1–Tg$. The first important information extracted from these thermal investigations is the drastic decrease of the glass transition temperature from 461 °C to 193 °C when the lead fluoride content increases from 0 to 60 mol% in the glass. It has been already shown that the glass transition temperature is strongly dependent on the network connectivity, which is related to the coordination number of the glass former and intermediary cations and the number of cross-linking bonds between the covalent chains. The starting tungsten phosphate glass with composition $60NaPO_3–40WO_3$ has already been described in the literature [4] and presents a high glass transition temperature and high viscosity related with the intermediary behavior of the WO_6 polyhedra. As previously discussed, these octahedral units are inserted in the phosphate chains of PO_4 tetrahedra and cross-link the metaphosphate chains, resulting in a highly connected glass network. Thus, the drastic decrease of glass transition temperatures with increasing lead fluoride content is a first indication that this highly connected network is being progressively modified and that the number of cross-linking covalent bonds also decrease. This lower connectivity can be due to the formation of terminal bonds such as P—F or W—F, replacing the bridging bonds P—O—P and W—O—W and/or a decrease of the coordination number of cations present in the oxide covalent network, i.e. phosphorus and tungsten. In these glasses, phosphorus can hardly change its geometry and it is assumed that it remains as tetrahedral PO_4 or PO_nF_m with $n + m = 4$. On the other hand, tungsten atoms commonly exhibit several coordination numbers in glasses. Particularly, it has been already shown that incorporation of large amounts of glass modifiers such as alkaline oxides or metallic fluorides in WO_3-based glasses result in a coordination change from 6 to 4 [27]. For this reason, these glasses present low viscosity and glass transition temperatures. These structural assumptions will be further discussed based on Raman results. Another important feature of the thermal data is the decrease of the glass thermal stability against devitrification for higher lead fluoride contents. Whereas the glass samples Pb0, Pb10 and Pb20 do not crystallize up to 550 °C, increasing PbF_2 contents from 30 to 60 mol% result in clear crystallization events at decreasing temperatures with a consequent lower thermal stability against devitrification, as listed in Table 1. This behavior explains the consequently lower glass forming ability and the spontaneous crystallization of melts for lead fluoride contents higher than 60%. Once again, it can be suggested that the less connected vitreous network with more terminal metal–fluorine bonds is less

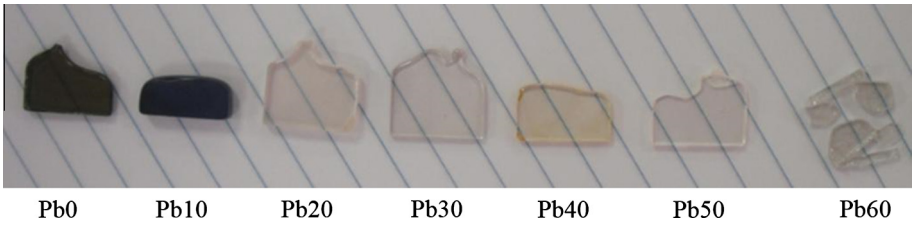

Fig. 1. Photograph of glass samples in the ternary system $(100 - x)[0.6NaPO_3–0.4WO_3]–xPbF_2$ with x ranging from 0 to 60.

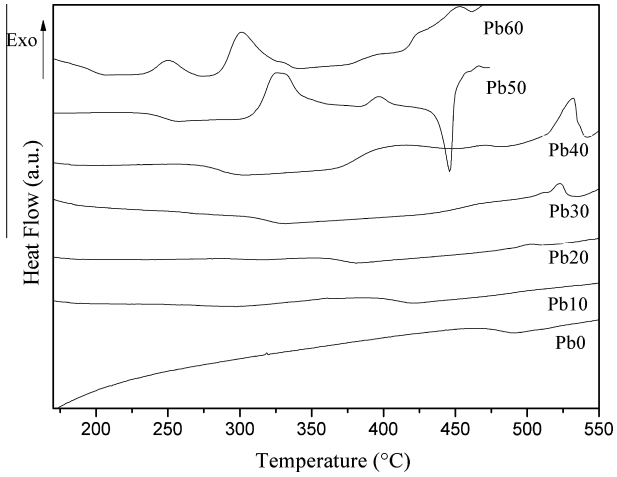

Fig. 2. DSC curves glass samples in the ternary system $(100 - x)[0.6NaPO_3–0.4WO_3]–xPbF_2$ with x ranging from 0 to 60.

viscous above Tg and consequently presents higher atomic diffusion with higher tendency for reorganization and crystallization.

UV–VIS absorption spectra recorded on the same glass samples were also used for bandgap energy Eg determination and the results are presented in Table 1. Lead fluoride incorporation induces an increase of Eg from 2.95 eV to 3.70 eV, which corresponds to a blue shift of the optical bandgap of about 80 nm. This higher UV transparency is related with a lower overall polarizability of the material and supports previous assumptions of an effective incorporation of PbF_2 in the tungsten phosphate glass network. The absorption spectra exhibit only absorption bands related with Eu^{3+} and therefore it was assumed that Eu^{2+} did not form in these glasses.

Raman spectra are shown in Fig. 3 for samples Pb0 to Pb60 together with the spectra of the crystalline references WO_3, $NaPO_3$ and Na_2PO_3F. The first important point to note is the lack of Raman bands at 1165 cm^{-1} and 688 cm^{-1}, observed in pure $NaPO_3$, for all glass samples. These bands are frequently reported in the literature and are attributed to stretching vibrations of terminal P—O bonds

Table 1
Glass compositions of glass samples in the ternary system $(100 - x)[0.6NaPO_3–0.4WO_3]–xPbF_2$, characteristic temperatures and optical bandgap energy.

Sample	Composition (mole%)			Characteristic temperatures (°C)				E (eV)
	$NaPO_3$	WO_3	PbF_2	Tg	Tx_1	Tc_1	$Tx_1–Tg$	
Pb0	60	40	0	461	–	–	–	2.95
Pb10	54	36	10	401	–	–	–	3.07
Pb20	48	32	20	361	–	–	–	3.20
Pb30	42	28	30	310	505	522	195	3.35
Pb40	36	24	40	275	368	406	93	3.48
Pb50	30	20	50	238	304	325	66	3.56
Pb60	24	16	60	193	232	250	39	3.70

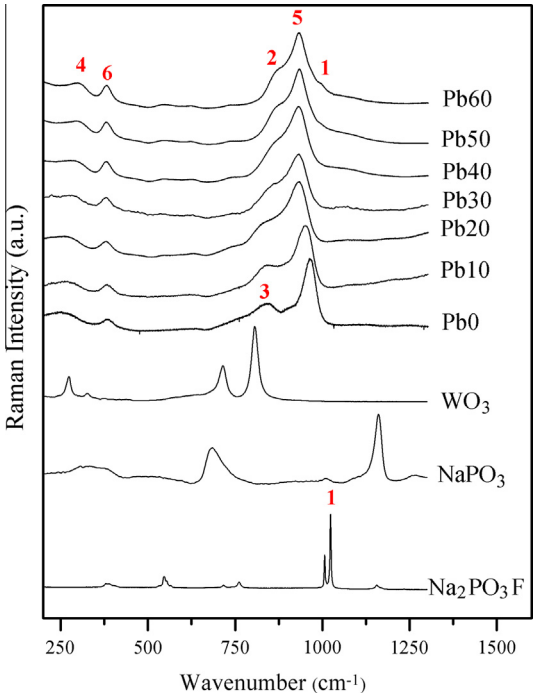

Fig. 3. Raman spectra of the glass samples in the ternary system $(100 - x)[0.6NaPO_3–0.4WO_3]–xPbF_2$ and the crystalline references WO_3, $NaPO_3$ and Na_2PO_3F.

and bridging P—O—P bonds in Q^2 tetrahedra respectively [3,28–30]. Thus, it can be assumed that pure metaphosphate structures built-up from chains of PO_4 tetrahedra are not present in the glass structure, according to the intermediary behavior of WO_3 (P—O—W bonds) and the modifier behavior of PbF_2 (P—F bonds). For PbF_2-free sample, tungsten oxide behaves as a glass intermediary since WO_6 octahedra are inserted inside the phosphate chains through P—O—W bonds, resulting in cross-linking bonds between the phosphate chains and higher network connectivity. The progressive network break with PbF_2 addition is also confirmed by two Raman bands centered at 1000 cm^{-1} (Band 1) and 865 cm^{-1} (Band 2) which are attributed to P—O stretchings in PO_3F and P$(O,F)_4$ units respectively [31,32]. Even for high lead fluoride contents, these Raman bands are weak because of the much higher intensity of tungsten related bonds. In fact, these bonds exhibit higher polarizabilities related with the high tungsten atomic number, resulting in intense Raman bands. Strong changes could also be detected around tungstate units. First, the Raman band 3 centered at 835 cm^{-1} and attributed to W—O—W stretching modes [33] progressively vanishes with increasing PbF_2 contents, suggesting that the bridging bonds between the WO_6 octahedra, and consequently the WO_6 clusters, also disappear. Previous works on alkaline tungsten oxyfluoride crystals identified W—F stretchings around 300 cm^{-1} [34]. In our materials, the weak Raman band labeled 4 which appears for higher lead fluoride contents has been

attributed to these tungsten fluorine vibrations and it is in agreement with the W—O—W rupture. Since it is proposed that fluorine progressively links to P and W, it is also suggested that the substituted oxygens migrate in the neighborhood of Pb^{2+} ions. Another important feature is the shift of the main Raman band labeled 5 from 965 cm^{-1} (W—O) for glass Pb0 to 930 cm^{-1} (W—F) for sample Pb60. This Raman band is characteristic of tungsten oxide compounds and is related with symmetric stretchings of terminal W—O bonds (W=O or W—O^-) [33]. A possible explanation for this shift could be a change of the tungsten coordination number from 6 to 4 as suggested earlier in this work. However, another band labeled 6 is observed in all samples and frustrates this first assumption. In fact, this band is due to deformation modes of WO_6 units in tungstate compounds and is a clear indication of the octahedral coordination of tungsten atoms. Thus, the observed shift is not related with a coordination change but it can be attributed to an increasing fluorine environment around these W—O bonds. Another important point explaining this shift is the replacement of Na^+ ions by Pb^{2+} near the W—O^- bonds for the charge balance. Finally, the higher intensity and narrowing of band 6 suggests a higher symmetry of the WO_6 units. Once again, this result is in agreement with the rupture of W—O—W bonds and a possible partial substitution of oxygen by fluorine in the WO_6 octahedra. All these Raman data are useful to depict a general structural model in which lead fluoride incorporation progressively depolymerizes the highly connected tungsten phosphate network through terminal P—F and some W—F bonds. Part of the W—O—W bridging bonds is replaced by W—F in the WO_6 octahedra, resulting in the progressive disappearance of the WO_6 clusters responsible of the partial reduction of tungsten atoms. For this reason, the dark coloration also vanishes. This modified tungsten lead fluorophosphate network is more ionic and less connected, justifying the lower glass transition temperatures and thermal stabilities against devitrification.

Glass samples were also heat-treated near the first crystallization temperature, in order to investigate which crystalline phases are formed during the devitrification process. These data can be helpful for additional structural information, as well as for possible optical applications. Heat-treatments were performed on samples Pb40, Pb50 and Pb60 because of clear crystallization events identified by DSC. As shown from Fig. 4, the glass Pb40 exhibited preferential precipitation of lead fluorophosphate $Pb_5F(PO_4)_3$ whereas cubic lead fluoride β-PbF_2 has been identified in sample Pb60. X-ray diffraction data for sample Pb50 are similar to those for Pb40 and are not presented in Fig. 4. These results bring two important information. First, some phosphate tetrahedra PO_4 are not modified by fluorine (formation of P—F bonds) in glasses Pb40 and Pb50 since PO_4^{3-} orthophosphate ions are identified in the crystalline phase. It can also be assumed that there are two kinds of fluorine atoms in these glasses: free fluoride anions F^- around the metallic cations Na^+ and Pb^{2+} which are precipitated in the crystalline phases $Pb_5F(PO_4)_3$ and β-PbF_2, and fluorine atoms linked to phosphorus and tungsten by covalent P—F and W—F bonds. These fluorine atoms probably remain in the glassy phase after crystallization. Besides the structural information extracted from these X-ray diffraction data, it must also be noted that precipitation of β-PbF_2 in the sample Pb60 is a very interesting result for future optical applications since lead fluoride is known to be a suitable host for luminescent rare earth ions, due to its very low phonon energy (~500 cm^{-1}). From this point of view, this sample looks promising for preparation of transparent RE-doped luminescent glass–ceramics.

Fig. 5 presents the emission spectra of the glasses excited at 393 nm. The characteristic transitions of Eu^{3+} in the range 570–720 nm are assigned for all bands. For the Pb0Eu sample which does not contain PbF_2, the bands around 535 nm (18,692 cm^{-1}) and 555 nm (18,018 cm^{-1}) most probably correspond to emission of W^{5+} and W^{4+} ions, since there is no Eu^{3+} state with these energies. In fact, these two bands also appear for the other samples but with considerably lower intensity as the presence of PbF_2 decreases the content of such tungsten species. From the spectra, we calculated the spontaneous emission coefficient (A_{RAD}), the radiative lifetime (τ_{RAD}), the quantum efficiency (q), and the Judd–Ofelt (Ω_2, Ω_4) parameters (Table 2). As the $^5D_0 \rightarrow {}^7F_1$ transition is purely magnetically dipolar, and its radiative rate does not depend on the local field imposed by the environment, this transition is often used as an internal standard to measure the relative intensities of the other transitions [35]. The relation $A_{0-\lambda} = A_{0-1}$ $(S_{0-\lambda}/S_{0-1})$ $(\sigma_\lambda/\sigma_1)$, where $S_{0-\lambda}$ is the area under the curve related to the $^5D_0 \rightarrow {}^7F_\lambda$ transition obtained from the spectral data, and σ_λ is the energy barycenter of the $0-\lambda$ transition, provides the $A_{0-\lambda}$ values. Here, we assumed that $A_{0-1} = 50\ s^{-1}$, as it is typical in the literature, and that the transitions $^5D_0 \rightarrow {}^7F_{5,6}$ have negligible intensities. Although the calculations of radiative rates were based on lanthanide complexes in solutions, they have been used for lanthanides doped in solid state matrices as a form to evaluate their luminescent properties [36–39]. The details of these calculations

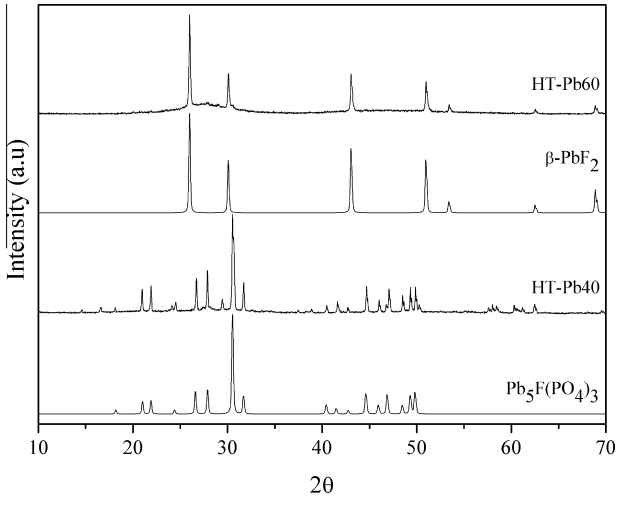

Fig. 4. X-ray diffraction patterns of heat-treated samples of composition $36NaPO_3$–$24WO_3$–$40PbF_2$ (Pb40), $24NaPO_3$–$16WO_3$–$60PbF_2$ (Pb60) and of the crystalline references β -PbF_2 and $Pb_5F(PO_4)_3$.

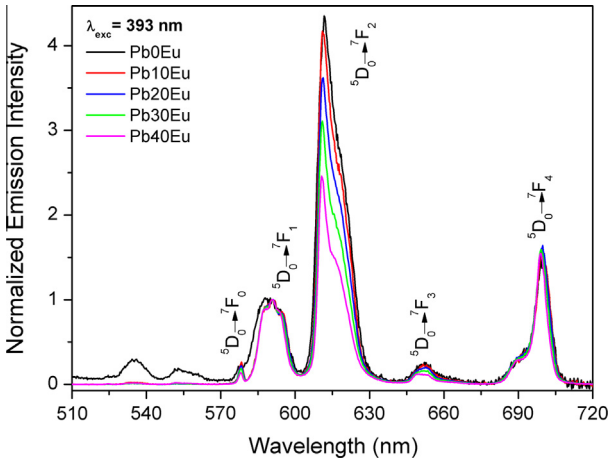

Fig. 5. Emission spectra of glass samples in the ternary system $(100 - x)[0.6NaPO_3$–$0.4WO_3]$–$xPbF_2$ doped with 0.1 mol% of Eu_2O_3 under excitation at 393 nm. The transitions from excited state $^5D_0$ are indicated near the bands.

Table 2
Optical parameters extracted from the Eu^{3+} emission spectra of glass samples in the ternary system $(100 - x)[0.6NaPO_3–0.4WO_3]–xPbF_2$ doped with 0.1 mol% of Eu_2O_3.

Sample	A_{RAD} (ms^{-1})	I_2/I_1	τ_{RAD} (ms)	τ_{exp} (ms)	q	$\Omega_2 \times 10^{-20}$ cm^2	$\Omega_4 \times 10^{-20}$ cm^2	n-OH	X (CIE)	Y (CIE)
Pb0Eu	0.31 ± 0.01	3.83	3.28 ± 0.16	0.92 ± 0.09	0.28 ± 0.03	3.50 ± 0.17	2.23 ± 0.11	0.33	0.628	0.365
Pb10Eu	0.33 ± 0.02	3.54	3.02 ± 0.15	1.02 ± 0.1	0.34 ± 0.03	3.75 ± 0.19	2.68 ± 0.13	0.03	0.671	0.327
Pb20Eu	0.30 ± 0.01	3.33	3.28 ± 0.16	1.78 ± 0.18	0.54 ± 0.05	3.26 ± 0.16	2.76 ± 0.14	0	0.672	0.326
Pb30Eu	0.27 ± 0.01	2.80	3.67 ± 0.18	1.95 ± 0.2	0.53 ± 0.05	2.75 ± 0.14	2.64 ± 0.13	0	0.667	0.329
Pb40Eu	0.23 ± 0.01	2.21	4.27 ± 0.21	2.27 ± 0.23	0.53 ± 0.05	2.16 ± 0.11	2.44 ± 0.12	0	0.666	0.333

are given by Werts et al. [40]. The $^5D_0$ radiative rates $A_{rad} = \Sigma(A_{0-J})$ were calculated and the experimental lifetime values were obtained by fitting the $^5D_0$ luminescence decay with $I = I_0 \exp(-t/\tau_{exp})$, as shown in Fig. 6 [41].

Luminescence data point out that incorporation of lead fluoride improves the quantum efficiency with a maximum value around 0.54 for PbF_2 contents above 20 mol%. Although the quantum efficiency doesn't further increase for higher contents, the local symmetry around Eu^{3+} ions is higher for the lead fluoride saturated samples, as suggested by the decrease in intensity ratio of $^5D_0 \rightarrow {}^7F_2/{}^5D_0 \rightarrow {}^7F_1$ transitions, and the slight increase in the intensity ratio $^5D_0 \rightarrow {}^7F_4/{}^5D_0 \rightarrow {}^7F_2$. In addition, by increasing the amount of fluoride ions the values of A_{RAD} and Ω_2 are decreased and the lifetime values significantly increase from 0.92 to 2.27 ms. Reisfeld and Jorgensen consider that Ω_2 indicates the covalence of the bond between the rare earth ion and the network; the larger the Ω_2, the more covalent the bond and the lower the symmetry around the ion [42]. Hence, the smaller Ω_2 values obtained for the most PbF_2 concentrated samples suggests an increased Eu^{3+} symmetry. Low Ω_2 and Ω_4 values also suggest that a weakly polarizable and rigid chemical environment is formed around Eu^{3+} [43]. Judd–Ofelt calculations also allowed evaluating the average number of hydroxyl groups OH in the Eu^{3+} vicinity, as presented in Table 2. In glasses with low lead fluoride contents (0% and 10%), some hydroxyl groups remain around Eu^{3+} ions whereas the presence of higher fluoride contents eliminate these functional groups leading to the improved emission properties earlier described [44]. The Eu^{3+} luminescence data are consistent with our previous structural description and point out a progressive change in the rare earth vicinity from oxide-like (with some hydroxyl groups) to a fluoride-like environment, resulting in a more symmetric neighborhood with lower local phonon energy and improved emission properties. The presence of Eu^{2+} cannot be totally excluded since the emission band detected around 440 nm could be related with both Eu^{2+} or tungstate luminescence.

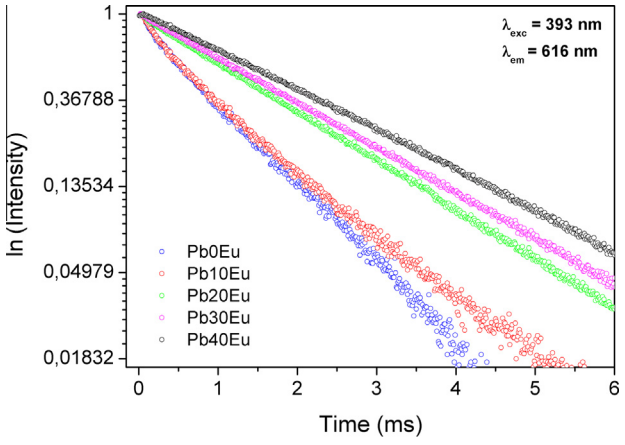

Fig. 6. Intensity decay profiles of glass samples in the ternary system $(100 - x)[0.6NaPO_3–0.4WO_3]–xPbF_2$ doped with 0.1 mol% of Eu_2O_3 at 612 nm under excitation at 393 nm.

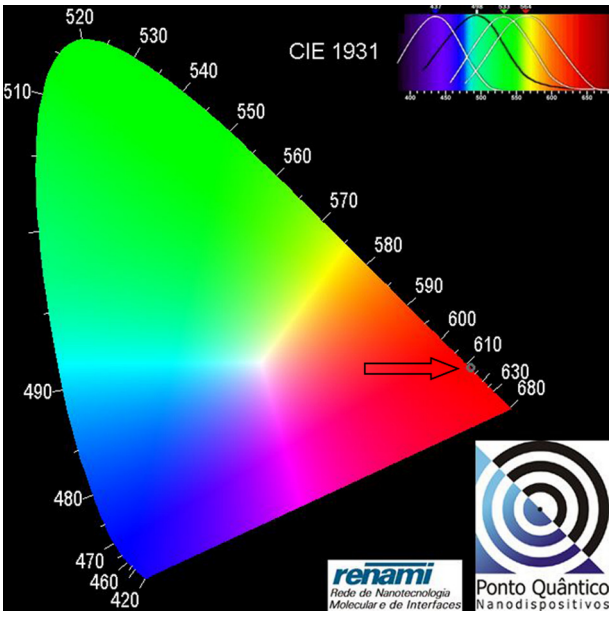

Fig. 7. Chromaticity coordinates calculated from emission spectra for glass composition $36NaPO_3–24WO_3–40PbF_2$ (Pb40), (λ_{exc} = 393 nm).

The most intense emission of Eu^{3+} at 610 nm favors saturated CIE chromaticity. We generated chromaticity coordinates for these samples using the software Spectra Lux 2.0 [45] and the respective emission spectra were recorded at room temperature. The CIE chromaticity coordinates of these lead fluoride tungsten phosphate glasses excited at 393 nm lie above the National Television Standard Committee (NTSC) standard values (x = 0.670 and y = 0.330) [46], indicating a possible application as a red-emitter phosphor (see Fig. 7).

4. Conclusion

Glass samples were prepared by the melt-quenching method in the ternary system $NaPO_3–WO_3–PbF_2$ with a constant $NaPO_3/WO_3$ ratio of 3/2 and increasing PbF_2 contents from 0 to 60 mol%. Increasing lead fluoride concentrations results in transparent and homogeneous glasses with lower glass transition temperatures (falling from 461 °C to 193 °C), lower thermal stability against devitrification and higher optical bandgap values. Raman data were useful to identify structural changes in the glass network which is progressively disrupted with terminal P—F and W—F bonds replacing bridging P—O—P and W—O—W linkages. Such a structural model is in agreement with the lower glass transition temperatures, glass thermal stability and higher optical bandgap, related with a higher ionic character of the glass network. It must be highlighted that Raman and crystallization suggest that two distinct fluorine atoms are present in the glass network. Some fluorine atoms link to phosphorus and tungsten and modify the glass structure. Another part of fluorine remains as lead fluoride rich domains

which crystallize under heat-treatment. Eu^{3+} doped glass samples with very good optical quality were also successfully prepared from lead fluoride contents from 0 to 40 mol% and the europium emission properties were shown to be dependent on composition. Radiative lifetime values, as well as quantum efficiencies, increase with higher fluoride content since the hydroxyl rich oxide environment at the Eu^{3+} siting is progressively replaced by a more symmetric and lower phonon energy fluoride vicinity, also identified from the variation in the intensity ratio of $^5D_0 \rightarrow {}^7F_2/{}^5D_0 \rightarrow {}^7F_1$ transitions. The results indicate that these glasses can be potentially used in bright red emitting devices.

Acknowledgments

The authors would like to thank the Brazilian funding agencies FAPEMIG, FAPESP (Cepid Project 2013/07793-6), FINEP, CNPq and CAPES for financial support of this work.

References

[1] C.C. Araujo, W. Strojek, L. Zhang, Structural studies of $NaPO_3$–WO_3 glasses by solid state NMR and Raman spectroscopy, J. Mater. Chem. Phys. 16 (32) (2006) 3277.
[2] G. Poirier, F.C. Cassanjes, Y. Messaddeq, Local order around tungsten atoms in tungstate fluorophosphate glasses by X-ray absorption spectroscopy, J. Non-Cryst. Sol. 351 (46–48) (2005) 3644.
[3] G. Poirier, Y. Messaddeq, S.J.L. Ribeiro, Structural study of tungstate fluorophosphates glasses by Raman and X-ray absorption spectroscopy, J. Sol. State Chem. 178 (5) (2005) 1533.
[4] G. Poirier, M. Poulain, Y. Messaddeq, New tungstate fluorophosphates glasses, J. Non-Cryst. Sol. 351 (4) (2005) 293.
[5] E.L. Falcao, C.B. Araujo, C.A.C. Bosco, Non linear optical properties of tungstate fluorophosphates glasses, J. Appl. Phys. 96 (5) (2004) 2525.
[6] G. Poirier, C.B. Araujo, Y. Messaddeq, Tungstate fluorophosphates glasses as optical limiters, J. Appl. Phys. 91 (12) (2002) 10221.
[7] G. Poirier, M. Nalin, Y. Messaddeq, Photochromic properties of tungstate-based glasses, Sol. State Ionics 178 (11–12) (2007) 871.
[8] G. Poirier, M. Nalin, L. Cescato, Bulk photochromism in a tungstate fluorophosphates glass: a new optical memory material?, J Chem. Phys. 125 (16) (2006) 161101.
[9] G. Poirier, F. Ottoboni, F.C. Cassanjes, Redox behavior of molybdenum and tungsten in phosphate glasses, J. Phys. Chem. B 112 (15) (2008) 4481.
[10] G. Poirier, V.A. Jerez, C.B. de Araújo, Y. Messaddeq, S.J.L. Ribeiro, M. Poulain, J. Appl. Phys. 93 (3) (2003) 1493–1497.
[11] M.J. Dejneka, The luminescence and structure of novel transparent oxyfluoride glass–ceramics, J. Non-Cryst. Solids 239 (1998) 149.
[12] V. Nazabal, S. Todoroki, S. Inoue, T. Matsumoto, S. Suehara, T. Hondo, T. Araki, T. Cardinal, Spectral properties of Er^{3+} doped oxyfluoride tellurite glasses, J. Non-Cryst. Solids 326 (2003) 359.
[13] S.A. Polishchuk, L.N. Ignateva, Y.V. Marchenko, V.M. Bouznik, Oxyfluoride glasses (a review), Glass. Phys. Chem. 37 (1) (2011) 1–20.
[14] J.L. Adam, Fluoride glass research in France, J. Fluorine Chem. 107 (2001) 265–270.
[15] M.J. Dejneka, Transparent oxyfluoride glass–ceramics, MRS Bull. 23 (11) (1998) 57–62.
[16] P.P. Fedorov, A.A. Luginnina, A.I. Popov, Transparent oxyfluoride glass–ceramics, J. Fluorine Chem. 172 (2015) 22–50.
[17] P.A. Tick, N.F. Borrelli, L.K. Cornelius, M.A. Newhouse, Transparent glass–ceramics for 1300 nm amplifier applications, J. Appl. Phys. 78 (1995) 6367–6375.
[18] M.J. Dejneka, The luminescence and structure of novel transparent oxyfluoride glass–ceramics, J. Non-Cryst. Solids 239 (1998) 149–155.
[19] T. Suzuki, S. Masaki, K. Mizuno, Y. Ohishi, Novel oxyfluoride glass and transparent glass–ceramics for fiber lasers and fiber amplifiers, Proc. SPIE 7721 (2010) 77210T.
[20] I. Gugov, M. Mueller, C. Ruessel, Transparent oxyfluoride glass–ceramics co-doped with Er^{3+} and Yb^{3+}-crystallization and upconversion spectroscopy, J. Solid State Chem. 184 (2011) 1001–1007.
[21] A.J. Stevenson, H. Serier-Brault, P. Gredin, M. Mortier, Fluoride materials for optical applications: single crystals, ceramics, glasses and glass–ceramics, J. Fluorine Chem. 132 (2011) 1165–1173.
[23] A. de Pablos-Martin, C. Patzig, T. Hoeche, A. Duran, M.J. Pascual, KLaF4 nanocrystallization in oxyfluoride glass–ceramics, Cryst. Eng. Comm. 15 (35) (2013) 6979–6985.
[24] H. Yu, H. Guo, M. Zhang, Y. Liu, M. Liu, L.J. Zhao, Distribution of Nd^{3+} ions in oxyfluoride glass–ceramics, Nanoscale Res. Lett. 7 (2012) 275.
[25] J. Tauc, in: Amorphous and Liquid Semi-Conductors, Plenum Press, New York, 1974 (Chapter 4).
[26] Powder diffraction file (PDF), International Centre for Diffraction Data-Joint Committee of Powder Diffraction Standards (ICDD-JCPDS), 2000.
[27] B.G. Aitken, M.J. Dejneka, US Patent 09/490653, 2000.
[28] M. Tatsumisago, Y. Kowada, T. Minami, Phys. Chem. Glasses 29 (1988) 63.
[29] S.H. Morgan, R.H. Magruder, J. Am. Ceram. Soc. 73 (1990) 753.
[30] B.N. Nelson, G.J. Exarhos, J. Chem. Phys. 71 (1979) 2739.
[31] L.Y. Zhang, H.T. Sun, H.T. Wu, Effects of PbF2 on the spectroscopic, lasing and structural properties of Yb^{3+}-doped fluorophosphate glass, Sol. State Commun. 135 (1–2) (2005) 150–154.
[32] R. Lebullenger, L.A.O. Nunes, A.C. Hernandes, Properties of glasses from fluoride to phosphate composition, J. Non-Cryst. Solids 284 (1–3) (2001) 55–60.
[33] T. Sekiya, N. Mochida, S. Ogawa, J. Non-Cryst. Solids 176 (1994) 105.
[34] A.N. Vtyurin, J.V. Gerasimova, A.S. Krylov, Vibrational spectroscopy of alkaline tungsten oxyfluoride crystals, J. Raman Spectrosc. 41 (12) (2010) 1784–1791.
[35] P.F.S. Perreira, J.M.A. Caiut, S.J.L. Ribeiro, Y. Messaddeq, K.J. Ciuffi, L.A. Rocha, E. F. Molina, E.J. Nassar, J. Lumin. 126 (2007) 378.
[36] L.A. Rocha, K.J. Ciuffi, H.C. Sacco, E.J. Nassar, Mater. Chem. Phys. 85 (2004) 245.
[37] B. Yan, Q.P. Li, Micropor. Mesopor. Mater. 196 (2014) 284.
[38] Y.-F. Shao, B. Yan, Micropor. Mesopor. Mater. 193 (2014) 85.
[39] E. Gibelli, J. Kai, E. Teotonio, M. Felinto, H. Brito, J. Photochem. Photobiol. A Chem. 251 (2013) 154.
[40] M.H. Werts, R.T.F. Jukes, J.W. Verhoeven, The emission spectrum and the radiative lifetime of Eu^{3+} in luminescent lanthanide complexes, Phys. Chem. Chem. Phys. 4 (2002) 1542–1548.
[41] A.P. Duarte, L. Mauline, M. Gressier, J. Dexpert-Ghys, C. Roques, J.M.A. Caiut, E. Deffune, D.C.G. Maia, I.Z. Carlos, A.A.P. Ferreira, S.J.L. Ribeiro, M.J. Menu, Langmuir 29 (2013) 5878.
[42] R. Reisfeld, E. Zigansky, M. Gaft, Mol. Phys. 102 (11–12) (2004) 1319–1330.
[43] J.G. Santos, J.D.L. Dutra, S. Alves, G.F. De Sá, N.B. Da Costa, R.O. Freire, J. Braz. Chem. Soc. 24 (2013) 236.
[44] M.R. Dousti, G. Poirier, A.S.S. de Camargo, Opt. Mater. 45 (2015) 185–190.
[45] P.A. Santa-Cruz, F.S. Teles, Spectra Lux Software, Ponto Quantico Nanodispositivos, 2003.
[46] L. Zhou, J. Huang, F. Gong, F.Y. Lan, Z. Tong, Z.J. Sun, J. Alloys Comp. 495 (2010) 268.